Rakenteiden Mekaniikka (Journal of Structural Mechanics)
Vol. 51, No 1, 2018, pp. 27–35
http://rakenteidenmekaniikka.journal.fi/index
https://doi.org/10.23998/rm.69204

VERTAISARVIOITU
KOLLEGIALT GRANSKAD
PEER-REVIEWED
www.tsv.fi/tunnus

Modeling the stress effect on the measurement of magnetostriction in electrical sheets under rotational magnetization

A. Belahcen, P. Rasilo, K. Fonteyn, R. Kouhia, D. Singh, and A. Arkkio

Summary. The magnetostriction in electrical steel under rotational magnetization is usually measured with cross-shaped samples. However, the inhomogeneity of the magnetization and stress in the sample might hinder the measured results. In this paper, we investigate this phenomenon by using a magneto-mechanically coupled energy-based model to simulate the sample in a single sheet tester measurement setup, and compare the simulations and measurements. The results show that some anomalies in the measured magnetostriction can be explained by the inhomogeneous magnetization in the sample and the form effect, which result in inhomogeneous stresses and thus affect the observed quantities. The validity of the model as well as the presented statements are ascertained through experiments on the single sheet tester. The backgrounds of the used modelization technique are also detailed.

Key words: electrical steel, magnetoelasticity, magnetostriction, rotating magnetic field, single sheet tester

Received 2 February 2018. Accepted 17 May 2018. Published online 16 August 2018.

Introduction

The magnetostriction in electrical steel is known to generate vibrations and acoustic noise in transformers and rotating electrical machines [1]. The data necessary to model this phenomenon are acquired either from unidirectional or bidirectional measurements either under externally applied mechanical stresses or in a stress-free state. Measurements were made with disc-shaped samples [2] and showed that the magnetostriction might present some anisotropy. However, the measurement of rotational properties of the electrical steel is usually carried out with a rotational single sheet tester, and in most cases, a cross-shaped sample is used. The modelling of magnetostriction is primordial not only because of its harmful effects e.g. on losses [3], but also because it can be used to damp the vibrations as in [4]. Most of the models of

[1]Corresponding author: anouar.belachen@aalto.fi

magnetostriction in steel do not account for the strong coupling between stress and magnetostriction and thus fail to spot out the phenomenon we observed in this work.

In this paper we investigate the rotational magnetostriction in cross-and disc-shaped samples through modelling and measurements. The model we present and use computes the magnetostriction, accounts for the stresses arising from it, and thus allows for accurate results. Our hypothesis is that a large part of the discrepancy between measured and expected magnetostriction is associated with the inhomogeneity of the magnetization in the sample, which combined with the sample geometry results in compressive stresses and thus increased and apparently anisotropic magnetostriction.

This paper is organized so that in section II we present the energy-based model of magnetoelasticity we are using and its implementation into in-house FE software. In section III we present the results from simulations and measurements and compare them and in section IV we present a thorough discussion on both the model and its results.

Magneto-mechanical model

Constitutive equations

The energy-based constitutive equations of the electrical steel have been derived from an appropriate representation of the Helmholtz free energy in terms of the magneto-mechanical invariants $I_1..I_6$ and some model parameters $\alpha_i;\ i = 0..6$ [5]:

$$\rho\psi = \frac{1}{2}\lambda I_1^2 + 2G I_2 + \frac{1}{2}\sum_{i=0}^{4}\left[\frac{g_i(I_1)}{i+1}\left(\frac{I_4}{B_{ref}^2}\right)^{i+1} I_4\right] + \frac{1}{2}\alpha_5 I_5 + \frac{1}{2}\alpha_6 I_6 \tag{1}$$

$$I_1 = tr(\boldsymbol{\varepsilon});\ I_2 = \frac{1}{2}tr(\boldsymbol{\varepsilon}^2);\ I_4 = \boldsymbol{B}\cdot\boldsymbol{B};\ I_5 = \boldsymbol{B}\cdot\boldsymbol{\varepsilon}\cdot\boldsymbol{B};\ I_6 = \boldsymbol{B}\cdot\boldsymbol{\varepsilon}^2\cdot\boldsymbol{B} \tag{2}$$

with λ being the first Lamé parameter, G the shear modulus of the material, ρ the mass density, ψ the energy density, and

$$g_0 = \frac{3}{4}\alpha_0 \exp\left(\frac{3}{4}I_1\right) - \frac{1}{3}\mu_0 - \alpha_5 \tag{3}$$

$$g_i = \frac{3(i+1)}{4}\alpha_i \exp\left(\frac{4(i+1)}{3}I_1\right);\quad i = 1..4 \tag{4}$$

$\boldsymbol{B}$ is the magnetic flux density and B_{ref} a reference value. This representation of the energy is based on empirical observations from unidirectional measurements of magnetostriction under different stresses and flux densities [6]. The magneto-mechanically coupled constitutive equations are derived from (1) and

$$\boldsymbol{\sigma} = \rho\sum_{i=1,i\neq 3}^{6}\frac{\partial\psi}{\partial I_i}\frac{\partial I_i}{\partial\boldsymbol{\varepsilon}} \text{ and } \boldsymbol{M} = \rho\sum_{i=1,i\neq 3}^{6}\frac{\partial\psi}{\partial I_i}\frac{\partial I_i}{\partial\boldsymbol{B}}. \tag{5}$$

where $\boldsymbol{\sigma}$ is the Cauchy stress tensor, $\boldsymbol{\varepsilon}$ the strain tensors and $\boldsymbol{M}$ the magnetization vector. An extensive derivation of the model and its equations is given in [7].

The model results in an explicitly coupled formulation for the total stress tensor $\boldsymbol{\tau}$ and the magnetic field strength vector $\boldsymbol{H}$ in terms of the magnetic flux density vector and the mechanical strain tensor:

$$\begin{aligned}\boldsymbol{\tau}(\boldsymbol{B},\boldsymbol{\varepsilon}) = {} & \lambda I_1 \boldsymbol{I} + \rho \tilde{\psi}_1(I_4)\boldsymbol{I} + 2G\boldsymbol{\varepsilon} + \mu_0^{-1}\left(\boldsymbol{B}\otimes\boldsymbol{B} - \frac{1}{2}(\boldsymbol{B}\cdot\boldsymbol{B})\boldsymbol{I}\right) + \\ & 2\rho\psi_4\left(\boldsymbol{B}\otimes\boldsymbol{B} - (\boldsymbol{B}\cdot\boldsymbol{B})\boldsymbol{I}\right) + \frac{\rho}{2}\alpha_5\left(\boldsymbol{B}\otimes\boldsymbol{B}\cdot\boldsymbol{\varepsilon} - (\boldsymbol{B}\cdot\boldsymbol{\varepsilon}\cdot\boldsymbol{B})\boldsymbol{I}\right) + \\ & \frac{\rho}{2}\alpha_6\left[\begin{array}{l}\boldsymbol{B}\otimes\boldsymbol{B} + \boldsymbol{B}\otimes\boldsymbol{B}\cdot\boldsymbol{\varepsilon}^2 - \\ (\boldsymbol{B}\cdot\boldsymbol{\varepsilon}^2\cdot\boldsymbol{B})\boldsymbol{I} + (\boldsymbol{B}\otimes\boldsymbol{B}\cdot\boldsymbol{\varepsilon} + \boldsymbol{\varepsilon}\cdot\boldsymbol{B}\otimes\boldsymbol{B})\end{array}\right]\end{aligned} \tag{6}$$

$$\boldsymbol{H}(\boldsymbol{B},\boldsymbol{\varepsilon}) = \mu_0^{-1}\boldsymbol{B} - 2\rho\psi_4\boldsymbol{B} - \frac{\rho}{2}\alpha^5\boldsymbol{B}\cdot\boldsymbol{\varepsilon} - \frac{\rho}{2}\alpha_5\boldsymbol{B}\cdot\boldsymbol{\varepsilon}^2 \tag{7}$$

In (6) and (7) $\tilde{\psi}_1$ and ψ_4 are used to shorten the notation

$$\tilde{\psi}_1 = \frac{1}{2\rho}\sum_{i=0}^{4}\frac{\partial g_i}{\partial I_1}I_4^{i+1} \quad \text{and} \quad \psi_4 = \frac{1}{2\rho}\sum_{i=0}^{4}\frac{g_i}{i+1}I_4^i \tag{8}$$

The parameters of the model have been identified from unidirectional measurements on M400-50A material [8]. The results of measurements and model output are shown in Fig. 1.

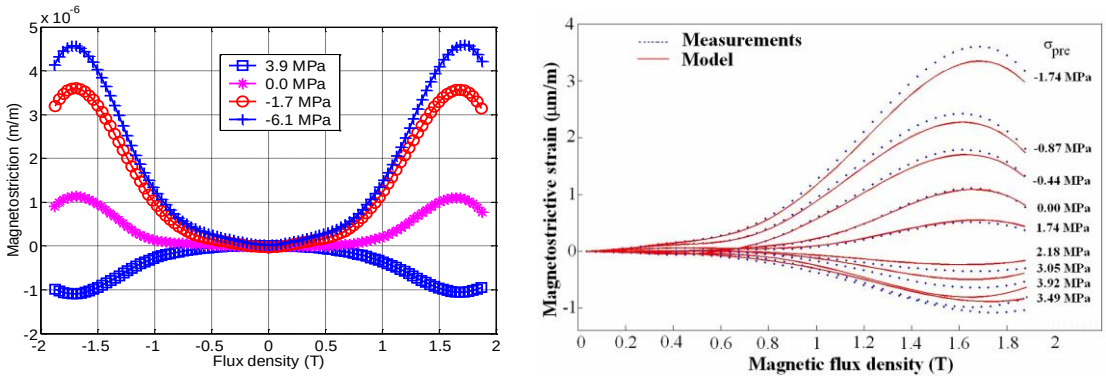

Figure 1. Measured magnetostrictive strains at different flux densities and applied mechanical stresses (left) and comparison with model prediction (right).

FE Implementation

The implementation of the magneto-mechanically coupled equations in FE was carried out with an in-house 2D software package, specially designed for the simulation of electrical machines and in which the field equations are coupled with the electrical

circuit equations of the machine windings. This approach makes it possible to feed the model from a voltage source. The software also implements the rotor motion and allows for time stepping analysis [9]. The coupled constitutive equations (6) and (7) were first linearized to the first order and then the weak form of the Galerkin method was applied to (6) and the principle of virtual work applied to (7), which resulted in [10]

$$\int_{\Omega}\left\{(\nabla\times w)\cdot\frac{\partial \boldsymbol{H}}{\partial \boldsymbol{B}}\Delta \boldsymbol{B}\right\}d\Omega+\int_{\Omega}\left\{(\nabla\times w)\cdot\frac{\partial \boldsymbol{H}}{\partial \boldsymbol{\varepsilon}}\Delta \boldsymbol{\varepsilon}\right\}d\Omega+\int_{\Omega}(\nabla\times w)\cdot\boldsymbol{H}_0\,d\Omega+\int_{\partial\Omega}w\cdot\boldsymbol{H}_0\,ds=0 \tag{9}$$

$$\int_{\Omega}\left\{\hat{\boldsymbol{\varepsilon}}^{\mathrm{T}}\frac{\partial \boldsymbol{\tau}}{\partial \boldsymbol{B}}\Delta \boldsymbol{B}\right\}d\Omega+\int_{\Omega}\left\{\hat{\boldsymbol{\varepsilon}}^{\mathrm{T}}\frac{\partial \boldsymbol{\tau}}{\partial \boldsymbol{\varepsilon}}\Delta \boldsymbol{\varepsilon}\right\}d\Omega+\int_{\Omega}\hat{\boldsymbol{\varepsilon}}^{\mathrm{T}}\boldsymbol{\tau}_0\,d\Omega-\int_{\Omega}\hat{\boldsymbol{u}}^{\mathrm{T}}(\boldsymbol{f}_{mech}+\boldsymbol{f}_{inert})d\Omega-\int_{\partial\Omega}\hat{\boldsymbol{u}}^{\mathrm{T}}\boldsymbol{f}_{surf}ds=0 \tag{10}$$

where w is a test or weight function and the quantities with hat are virtual ones. $\boldsymbol{u}$ is the mechanical displacement vector and $\boldsymbol{f}_{mech}$, $\boldsymbol{f}_{inert}$, $\boldsymbol{f}_{surf}$ are respectively mechanical, inertia body forces and surface forces. In the implementation, the shape functions of the finite element approximation are used as weight functions.

Equations (9) and (10) have been spatially discretized using standard finite element procedure and inserted into the in-house code, thus replacing the nonlinear model of iron core, which was previously based on the expression of the reluctivity as cubic spline of the square of flux density. The insertion of these equations in the code did not affected the electromagnetic coupling as this latter one takes place in the windings and conducting regions only whereas the magneto-mechanical coupling takes place in non-conducting iron.

Simulations and measurement results

Cross-shaped Sample

The cross-shaped sample used in the rotational single sheet tester has been simulated with the above FE approach, where the magnetic flux density has been set by adequate boundary conditions at each time step. Due to symmetry reasons, only half of the sample needs to be modeled. The magnetic boundary conditions were set as to obtain a flux density in the middle of the sample as close to the measured one as possible. However, some differences could not be avoided as seen later.

The computed flux density distribution in the sample and the deformation at the instant of time where the flux is at -45 deg. to the *x*-axis are shown in Fig. 2. The computed *xx*- and *yy*-stress components in the sample at the same instant of time and expressed in the *xy*-coordinate system are shown in Fig. 3, where remarkable residual stresses are observed. These stresses are due to the combined effect of the field inhomogeneity and the shape of the sample. Further, strong tensile stresses are observed at the sharp angles of the sample. These latter ones can be reduced by proper rounding of the corners.

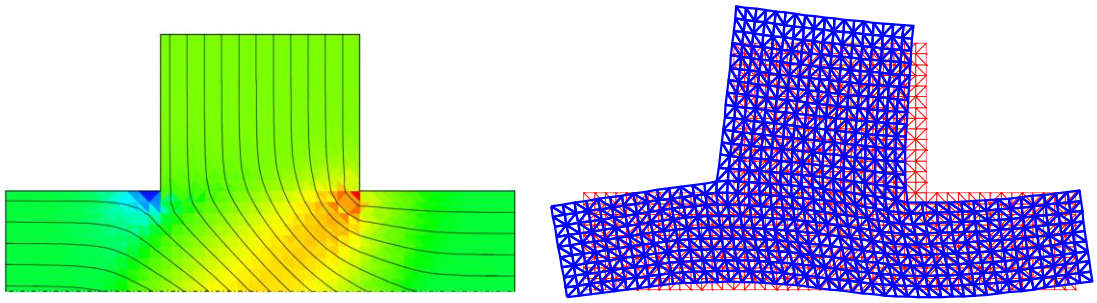

Figure 2. Computed magnetic flux density in the sample (right) and magnified deformation (left). The sample was fed by adequate fluxes in *x*- and *y*-direction.

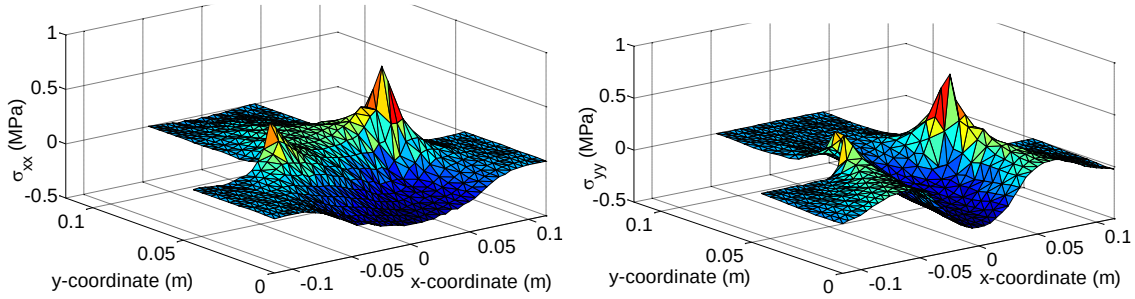

Figure 3. Computed *xx*- (left) and *yy*- (right) components of the stress in the *xy*-coordinate system. The inhomogeneous flux density distribution and the shape of the sample are responsible for the inhomogeneous stress distribution.

Disc-Shaped Sample

To prove that the inhomogeneous stress distribution in the cross-shaped sample was due to the above-mentioned inhomogeneity, we carried out similar simulation for a hypothetical disc-shaped sample. In this case, the flux density could be set homogeneously in the sample, and thanks to the regular shape, the form-effect does not produce any additional stress or strain inhomogeneity.

The computed deformation of the disc-sample at two different instants of time is shown in Fig. 4. The computed flux density distributions and the stress components corresponding to these times are not show as the flux densities are simply homogeneous and equal to the desired set value and the stress components are homogeneous and identically equal to zero. This result is in accordance with the general knowledge of how a disc deforms under homogeneous strains. In all computations, the mechanical boundary condition was set at the centre of the sample only as to keep it non-displaced while all the other nodes of the geometry were free to move.

Comparison with measurements

To validate the previous computations, measurements have been conducted on a cross-shaped sample magnetized by a rotational field single sheet tester. Figure 5 shows a photo of the magnetizing core where the sample has been inserted as well as the

instrumented middle part of the sample. At the middle of the sample and 20 mm apart from each other, four holes have been drilled to insert two 2-turns B-coils for the measurement of the two flux density components. Two rosette strain gages have also been glued at the middle of the sample from both sides for strain measurements and compensation of the bending of the sample. Above the strain gage, on one side of the sample, a 2-directional H-coil with 1000 turns for each direction has been positioned too for measuring the magnetic field strength components. The magnetizing coils of the device were fed from a computer-controlled power amplifier in view of rotational magnetic flux density in the sample. Figure 6 (left) shows the components of the measured strain tensor in the *xy*-coordinates as functions of the measured *x*-component of the magnetic flux density. The insert shows the locus of the rotational magnetic flux density. The simulated results for the same condition are shown in Fig. 6 (right). It could be seen that in the simulations the magnetic flux density is rather rectangular while in the measurement it is more circular. This fact is seen also as a difference in the shapes of the simulated and measured strain tensors. Figure 7 shows the computed result for the hypothetic disc-shaped sample. In this case, a smooth behaviour of all components is observed as no residual stresses are left in the sample and the filed locus is perfectly circular.

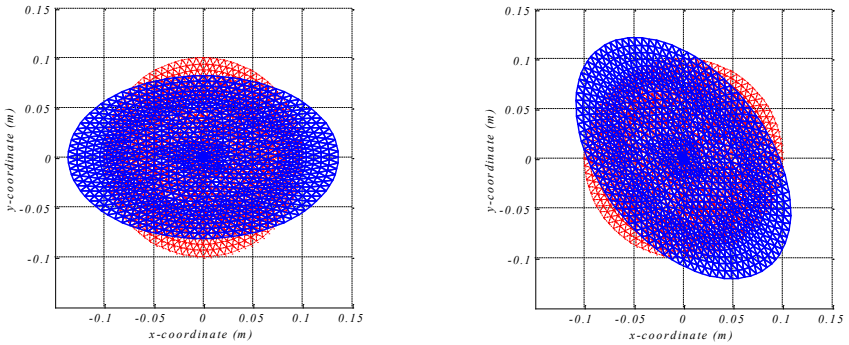

Figure 4. Computed deformations of the disc-shaped sample at two different orientations of the magnetic flux density. Thanks to the homogeneity of the field and the regular shape of the sample, the deformations are similar and follow the direction of the magnetic flux density.

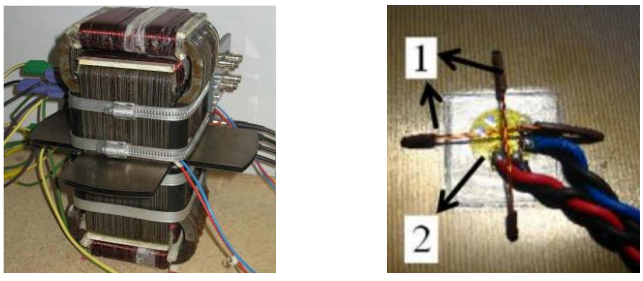

Figure 5. Photo of the rotational single sheet tester and details of the instrumented middle part of the sample. Strain gages are glued on both sides of the sample to compensate for the bending of the sample.

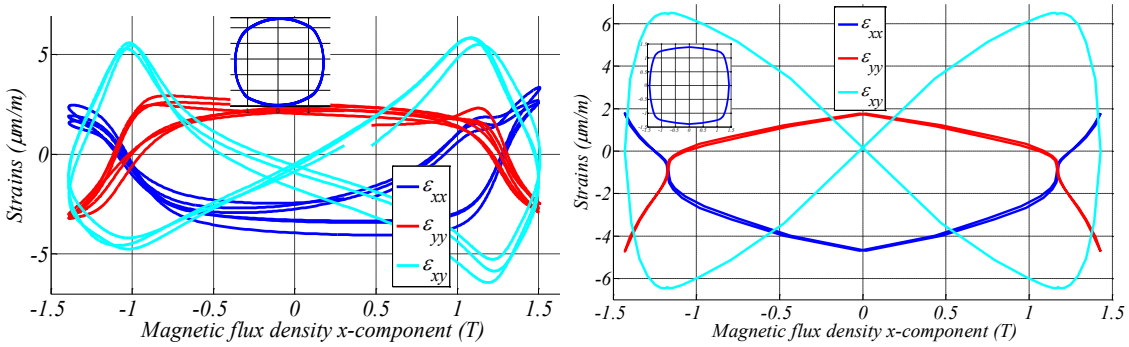

Figure 6. Measured (left) and computed (right) strain components in the cross-shaped sample as functions of the *x*-component of the magnetic flux density in the middle region of the sample. The inserts show the locus of the flux density vector in each case.

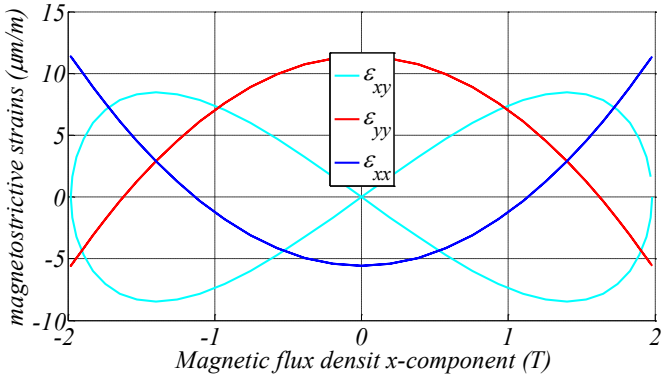

Figure 7. Computed strain components in the disc-shaped sample as functions of the computed *x*-component of the magnetic flux density.

Discussion

The presented coupled constitutive equations of electrical steel are based on energy considerations and thus have a sound thermodynamic meaning. These equations account for the well-known stress dependency of the magnetostrictive strains as well as the dependency of the magnetization on the stress also known as Villari-effect. However, it should be mentioned that the observed Villari-effect in the material we are dealing with is rather moderate contrary to some other materials as reported in [11]. The constitutive equations by themselves cannot model the deformation of magnetic structures with complex shapes. For this reason, the implementation of these equations into FE analysis and the simultaneous solution of the magnetic field and displacements are necessary. Such an implementation makes it possible to account for the stresses arising from different parts of the structure. The final state of the deformation is then defined by the energy equilibrium in the whole structure and not only in part of it.

The simulated results from the cross-shaped sample show that the form effect is very strong. This is seen in the stress distributions of Figs. 3 and 4. By shape effect, we mean

here the fact that the non-regular boundaries of the sample prohibit it from completely expanding under a mechanical strain load as the one due to magnetostrictive strains. Furthermore, the simulations show that the flux density distribution in this sample, although homogeneous at the centre of the sample, is not completely homogeneous in the whole sample. Such inhomogeneity results in inhomogeneous magnetostrictive strains, which are then observed at the centre of the sample as different from the expected strains. These expected strains are the ones computed for the disc-shaped sample as here the field and the strains are homogeneous and the structure is so that it expands freely under any homogeneous strain load.

The magnetostrictive strains measured and computed at the centre of the cross-shaped sample are quite similar to each other. This proves that the model we are using is appropriate for the purpose of magneto-mechanical analysis. Some differences can be also seen between the measurements and the computations. These differences are explained partly by the imposed locus of the magnetic flux density. In the measurements the control of the magnetic flux density makes this locus almost circular whereas in the computations the locus is almost square. The control of the flux density in the computations would require many iterations. A misalignment of the strain gages with respect to the B-coils is also present in the measurement set up as well as some harmonics that distort the results. A certain amount of anisotropy is also responsible for the asymmetry of the measured magnetostriction.

Conclusion

The methodology presented here suggests that one should be careful with the shapes of samples used in magnetic material characterization. The methodology has also been applied earlier to electrical machines. The effect of hysteresis, bidirectional stress loading, and anisotropy should be investigated in future works.

References

[1] A. Belahcen, "Vibrations of rotating electrical machines due to magnetomechanical coupling and magnetostriction," IEEE Trans. Magn., vol. 42, no. 4, pp. 971-974, Apr. 2006. https://doi.org/10.1109/TMAG.2006.871469.

[2] S. Somkun, A. J. Moses, P. I. Anderson, "Magnetostriction anisotropy and rotational magnetostriction of a nonoriented electrical steel," IEEE Trans. Magn., vol. 46, no. 2, pp. 302-305, Feb. 2010. https://doi.org/10.1109/TMAG.2009.2033123.

[3] M. LoBue, C. Sasso, V. Basso, F. Fiorillo, and G. Bertotti, "Power losses and magnetization process in Fe-Si nonoriented steels under tensile and compressive stress," J. Magn. Magn. Mater., no. 215–216, pp.124–126, 2000. https://doi.org/10.1016/S0304-8853(00)00092-5

[4] A. Shahaj, S. D. Garvey, "A possible method for magneto-strictive reduction of vibration in large electrical machines," IEEE Trans. Magn., vol. 47, no. 2, pp. 374-385, Feb. 2011. https://doi.org/10.1109/TMAG.2010.2095875

[5] A. Belahcen, K. Fonteyn, A. Hannukainen, and R. Kouhia, “On numerical modeling of coupled magnetoelastic problem,” in Proc. 21st Nordic Seminar on Computational Mechanics, Trondheim, Norway, 2008, pp. 203–206.
[6] A. Belahcen, M. El Amri, “Measurement of stress-dependent magnetisation and magnetostriction of electrical steel sheets,” in Proc of ICEM, Cracow, Poland, 2004, 4 p.
[7] K. A. Fonteyn, Energy-based magneto-mechanical model for electrical steel sheets, PhD. dissertation, Aalto University, Finland, 2010. https://aaltodoc.aalto.fi/handle/123456789/4808
[8] K. A. Fonteyn, A. Belahcen, P. Rasilo, R. Kouhia, and A. Arkkio, “Simulated results and experimental verification of a novel magneto- mechanical coupled method,” in Proc. ICEMS 2010, pp.1743-1748. http://ieeexplore.ieee.org/stamp/stamp.jsp?tp=&arnumber=5664490&isnumber=5662269
[9] A. Arkkio, Analysis of induction motors based on the numerical solution of the magnetic field and circuit equations, PhD. dissertation, Helsinki University of Technology, Espoo, Finland, 1987. https://aaltodoc.aalto.fi/handle/123456789/2158
[10] K. Fonteyn, A. Belahcen, R. Kouhia, P. Rasilo, A. Arkkio, “FEM for directly coupled magneto-mechanical phenomena in electrical machines,” IEEE Trans. Magn., vol. 46, no. 8, pp. 2923-2926, Aug. 2010. https://doi.org/10.1109/TMAG.2010.2044148
[11] Y. Kai, Y. Tsuchida, T. Todaka, M. Enokizono, “Influence of stress on vector magnetic property under rotating magnetic flux conditions,” IEEE Trans. Magn., vol. 48, no. 4, pp. 1421-1424, Apr. 2012. https://doi.org/10.1109/TMAG.2011.2173756

Anouar Belahcen, Katarzyna Fonteyn, Deepak Singh, Antero Arkkio
Aalto University, Dept. of Electrical Engineering and Automation
P.O.Box 15500, 00076-Aalto, Finland
anouar.belahcen@aalto.fi

Paavo Rasilo
Tampere University of Technology, Laboratory of Electrical Energy Engineering
FI-33101, Tampere, Finland
paavo.rasilo@tut.fi

Reijo Kouhia
Tampere University of Technology, Laboratory of Civil Engineering
FI-33101, Tampere, Finland
reijo.kouhia@tut.fi